Supplementary material

S.1 Low-frequency change in the IAS from historical observations

We examined the SST trends across the IAS in four monthly gridded instrumental datasets (Table 1). While the sources of raw input observations are generally the same, or very close to the same (International Comprehensive Ocean-Atmosphere Data Set [ICOADS]; Woodruff *et al.* 1987), the processing and interpolation methods differ between the data sets, and can be found in the corresponding reference given in Table 1. The temporal coverage for each data set also differs, so we use the longest possible common analysis period (1870-2013), and a common climatological base period of 1951-1980 relative to which we compute anomalies. Thus, the four instrumental data sets analyzed are not independent, but can be used to highlight uncertainty due to methodology such as quality control, measurement corrections, and interpolation schemes.

To highlight regions of agreement and disagreement, a "super-ensemble" is computed simply by interpolating each of the four data sets to a common 1° latitude by 1° longitude grid (*i.e.,* the native grid of the HadISST1 product), and computing an average SST field for each month between 1870-2013. We can calculate the linear trend field of this super-ensemble SST product, and detect areas of disagreement by masking 1° by 1° grid cells where some threshold number of the original products disagree on the sign of the trend (Fig. 4 [main text]). The individual SST products (and the super-ensemble) agree on a broad warming across the western tropical Atlantic and Caribbean Sea by ~0.4°C per century, with the greatest warming found along the northern coast of

South America in the southern Caribbean Sea. This warming is quite robust and certainly emerges from the background multidecadal variability seen in decadal smoothed time series of SST from the individual products as well as the super-ensemble mean (Figs. SF2-3). Mechanisms for the ~0.5°C per century warming along the northern coast of South America warrant further investigation, but it might be hypothesized that changes in zonal winds such as those associated with the CLLJ, which are linked to SST by meridional Ekman transport, are important.

Over the GoM, the only features shared by all four data sets (Fig. 4 [main text]) are a ring of warming along the west coast of Mexico to Louisiana, transitioning to a cooling along the coast from Louisiana to the southwestern tip of Florida (and along the east coast of Florida northward through South Carolina). Near the center of the GoM (see box indicated in Fig. 4b [main text] or Fig. SF1a), the rates of warming and the amplitude of cyclic multidecadal variability differ between products (Fig. SF2). For instance, the COBE2 product shows a nearly 1°C warming over this period, while the KaplanSST2 product shows effectively zero trend. Of particular relevance to recent and ongoing observational efforts is that the SST values even within the last century or two in the GoM are highly divergent between the four data sets, varying by ~0.5°C relative to their 1951-1980 base periods. To summarize, our current best estimates of SST warming in the Caribbean Sea robustly point to a ~0.8°C warming since the early 1900s, superimposed upon a clear multidecadal signal, while linear SST trends in the GoM are highly uncertain due in part to different treatments of raw historical observations, including in very recent years.

Short name	Begin	End	Spatial res.	Reference
HadISST1	01/1870	04/2014	1°	Rayner *et al.* (2003)
KaplanSST2	01/1856	05/2014	5°	Kaplan *et al.* (1998)
ERSST3b	01/1854	05/2014	2°	Smith *et al.* (2008)
COBE2	01/1850	12/2013	1°	Hirahara *et al.* (2014)

Table S1. List of instrumental sea surface temperature (SST) data sets used in this section and some essential characteristics. All data sets are monthly mean temporal resolution, and spatially interpolated using the methods described in the reference listed. A common base period of 1951–1980 is used for computing anomalies in each data set.

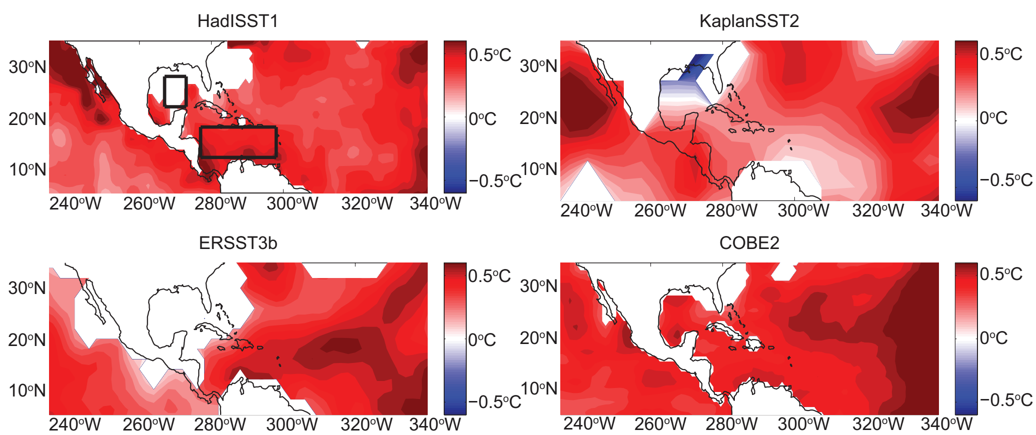

Figure SF1: Linear trends in SST (°C per century) from the four data sets on their native grids as listed in Table S1 using the common period of 1870-2013. Note that some grid cells with coarser resolution (e.g. Kaplan) will extend over land even though their values represent strictly ocean quantities.

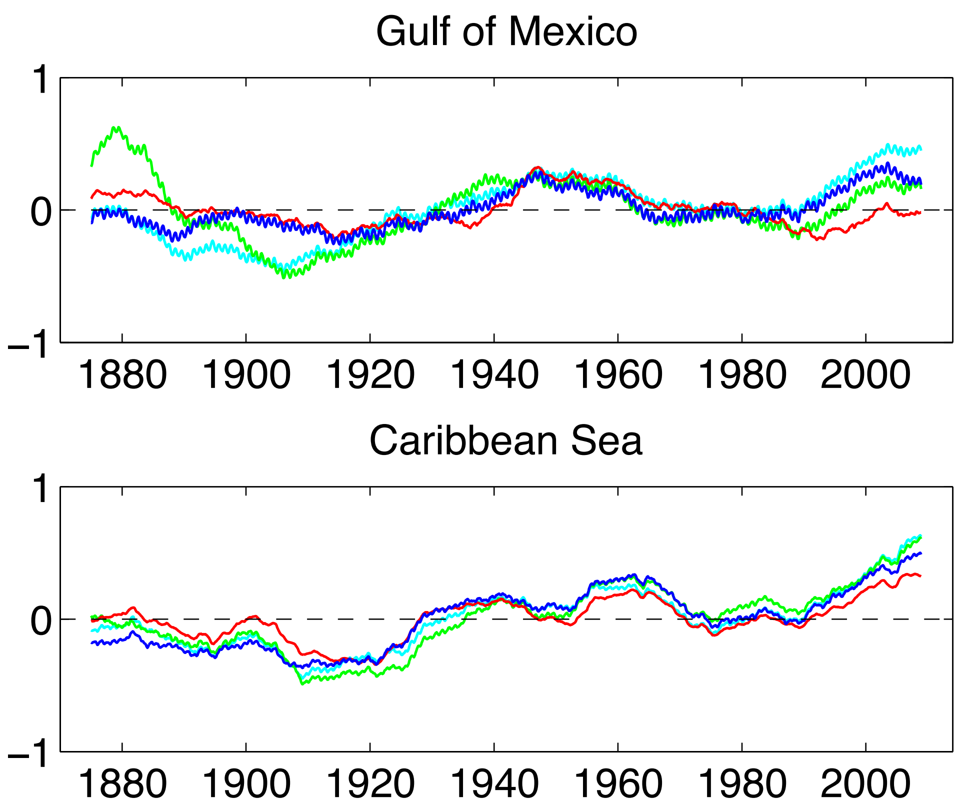

Figure SF2: Decadal smoothed time series of SST averaged over the GoM and Caribbean Sea boxes shown in Fig. 4 (main text) from each of the four instrumental SST data sets listed in Table 1. Colors are blue=HadISST1, red=KaplanSST2, green=ERSST3b, and cyan=COBE2.

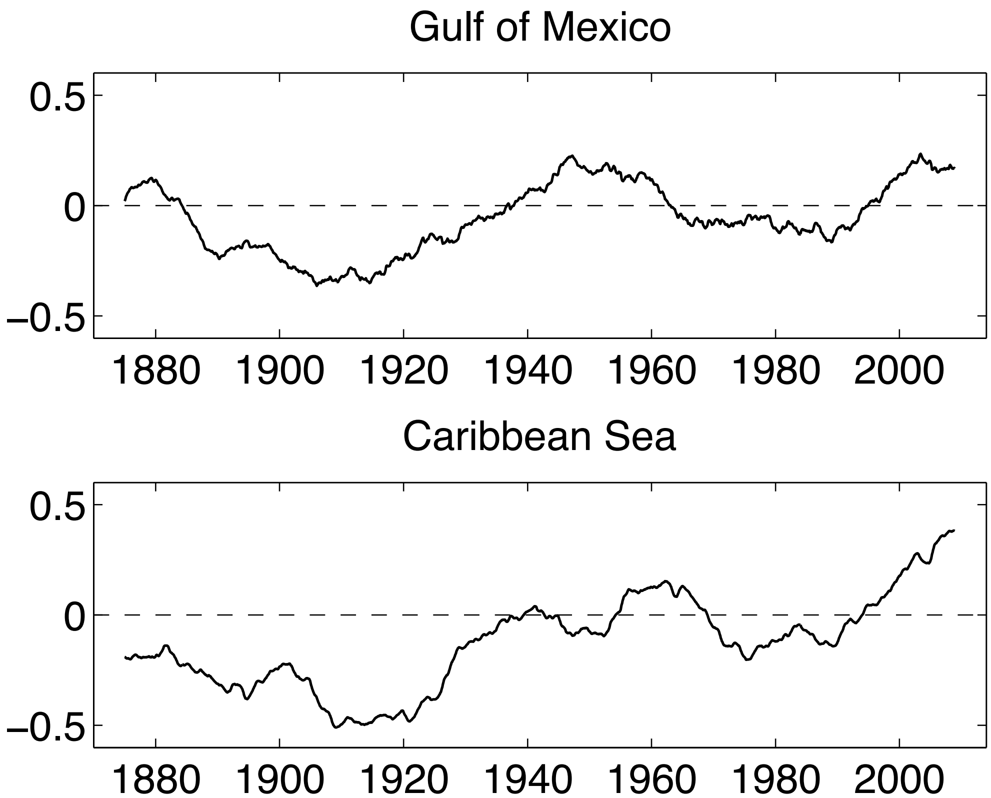

Figure SF3: Decadal smoothed time series of SST averaged over the GoM and Caribbean Sea boxes shown in Fig. 4 (main text) from the super-ensemble SST product (*i.e.*, the average of the three gridded products listed in Table 1).

S.2 The North American Monsoon Variability

About half of the gulf surges past Empalme, Mexico are related to the passage of a TC near the mouth of the Gulf of California (Douglas and Leal 2003; Higgins and Shi 2005). Consistent with these earlier studies, Hu and Dominguez (2015) find that the most intense precipitation over the NAM region occurs towards the end on the season, with moisture originating in the Gulf of California and tropical eastern Pacific in association with tropical cyclones (TCs). East Pacific easterly waves also support NAM events through gulf surges (Stensrud et al. 1997; Fuller and Stensrud 2000; Lang et al. 2007; Seastrand et al. 2014).

Numerous studies have documented a significant modulation of East Pacific, Caribbean, and GoM TC activity and tracks by the local manifestation of the MJO (e.g. Molinari et al. 1997; Maloney and Hartmann 2000a,b; Higgins and Shi 2001; Aiyyer and Molinari 2008; Jiang et al. 2012; Klotzbach 2014; Crosbie and Serra 2014). In particular, the GoM and western Caribbean hurricane genesis is four times more likely when the MJO phases associated with enhanced convection and low-level westerly flow are occurring in the IAS region as opposed to when the MJO is in its easterly phase over the region (Maloney and Hartmann 2000b). In addition east Pacific storm tracks, including easterly waves and TCs, are shifted closer to the west coast of Mexico during this time (Aiyyer and Molinari 2008; Crosbie and Serra 2014). Enhanced barotropic energy conversions and diabatic enhancement of eddies also occur during the convectively active phase of the MJO in the east Pacific, contributing to easterly wave growth in the region (Maloney and Hartmann 2000b; Aiyyer and Molinari 2008; Serra et al. 2010; Crosbie and Serra 2014).

S.3 Mesoscale eddies of the Caribbean Sea

Cold SSTs also appear west and north, ~1000 km away from the main upwelling areas of the Caribbean Sea (Fig. 7 of main text). Although there is a dynamical connection between the cold waters near-shore and offshore, upper ocean heat balance suggests that cold conditions offshore cannot be explained completely by the direct effect of Ekman transport away from the coast or geostrophic advection by the Caribbean Current (Jouanno and Sheinbaum 2013). Instead, model results suggest that intense mesoscale eddies in the Colombia Basin significantly shape turbulent cooling of the SSTs

(Fig. SF4). Vertical shear, turbulent heat fluxes, and surface cooling are increased at the location of jets that form on the downstream front of the eddies (Fig. SF4). The energy of the Caribbean eddies is known to vary semi-annually and interannually in response to variations of the CLLJ, through modulation of the westward Caribbean Current and instability processes (Jouanno et al. 2012), but their impact on the interannual variability of the upwelling system remains an open question.

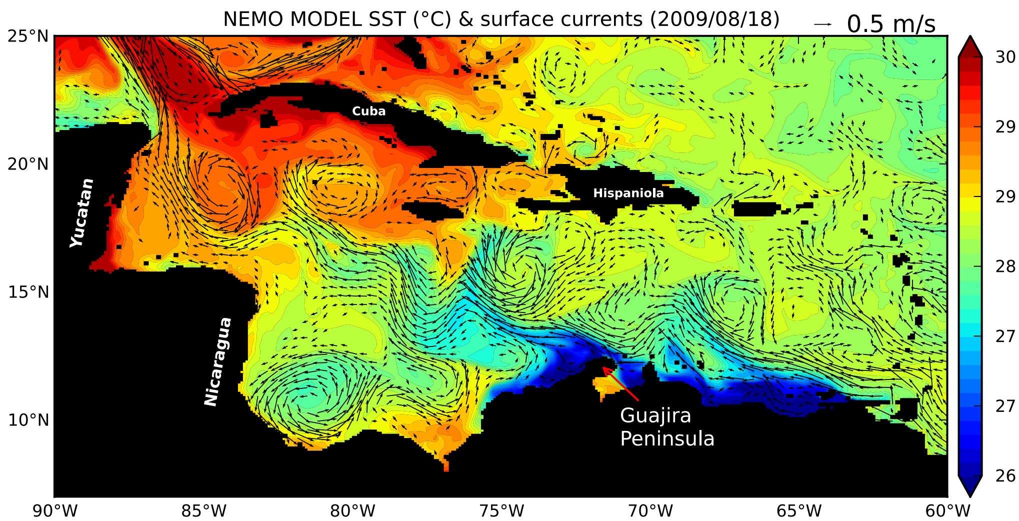

Figure SF4: Sea surface temperature and surface currents on 18th August 2009 from an IAS configuration of the model NEMO (Jouanno et al. 2012). It illustrates the interaction between mesoscale eddies and upwelling in the southern Caribbean. Surface current vectors are only shown for speeds greater than 0.15 m s^{-1}.

S.4: Uncertainty in ocean circulation in the IAS

Initial measurements of the Yucatan flow during 1999-2001 yielded a mean transport of ~23 Sv (Sheinbaum et al. 2002), which was substantially lower than the expected value of 28 Sv from historical hydrographic observations. A few years of measurements (2008-2013) though not always covering the whole Yucatan Channel suggest transport variations larger than 2-3 Sv. These are consistent with transport estimates based on a proxy using sea level differences across Yucatan (Fig. SF5) as well as surface geostrophic anomalies based on high-resolution along-track data of Northwest Providence and Old Bahama channels (Athie, et al. 2015).

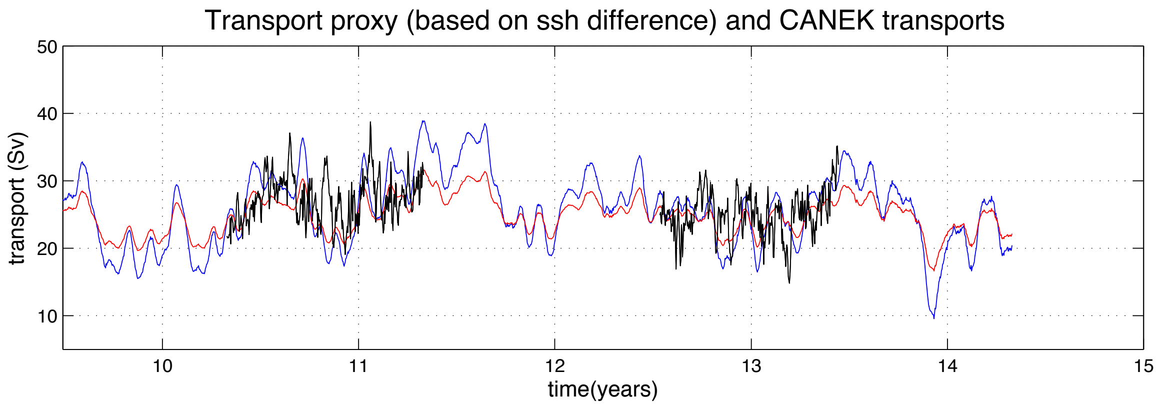

Figure SF5: Yucatan transports time-series (black) and proxy time-series based on regression between Canek transports and AVISO sea-level differences across the channel using 120 day (red) and 360 day (blue) averaged data.

S.5 Atmospheric sensitivity to Caribbean upwelling in the IAS

Although the influence of the Atlantic Warm Pool (AWP) on the atmosphere has been greatly documented in the past years, few studies have focused on the particular contribution of the southern Caribbean upwelling. There has been no study on its large-scale impact and there is still no consensus concerning its influence on the regional atmospheric circulation.

Preliminary results from regional simulations obtained with the Weather Research and Forecasting model (WRF; Skamarock et al., 2008) highlight that the coastal upwelling impacts significantly the atmospheric circulation over the whole IAS. Although the simulation slightly overestimates the rainfall amount in the IAS region, it reproduces the spatial distribution of the trade winds and precipitation reasonably well (Figs. SF6a and b).

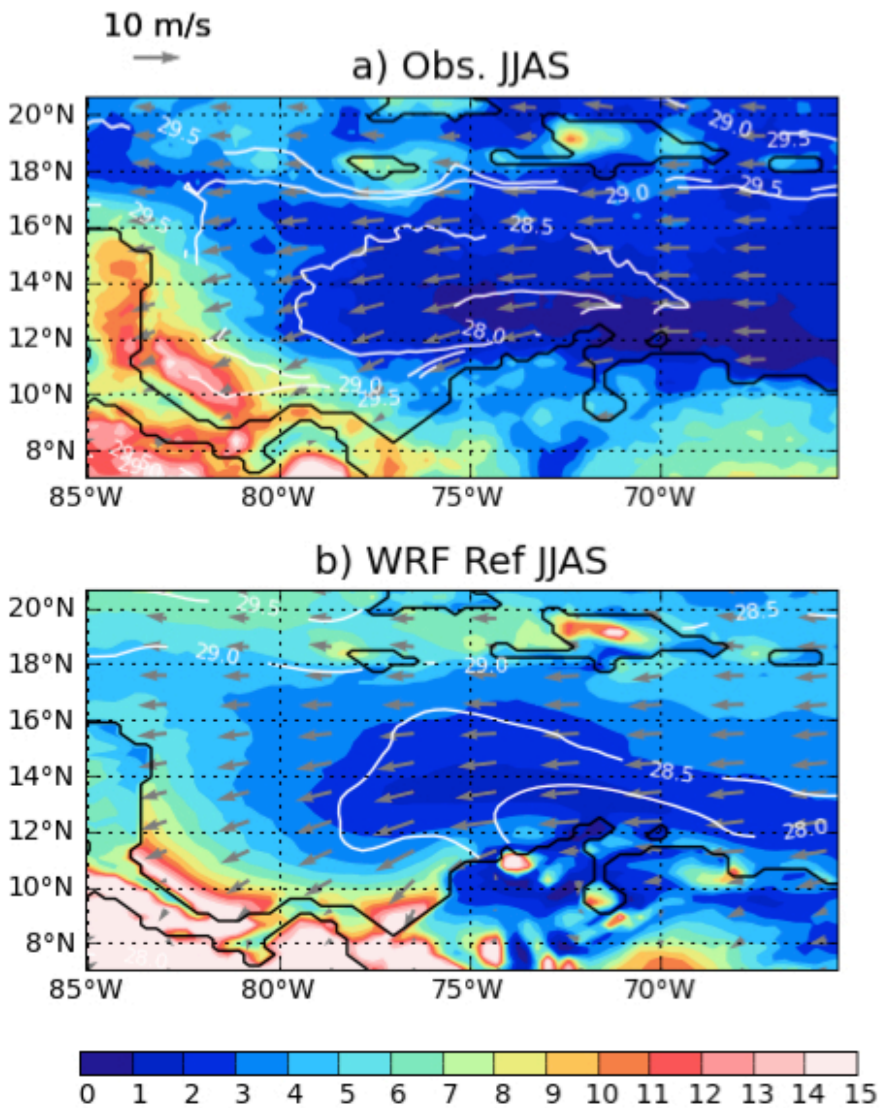

Figure SF6: Mean summer (JJAS) composite (2002-2008) of precipitation [shading; mm/day], SST [contours; °C] and 10-m wind [arrows; m/s] from a) TRMM, TMI and QuikSCAT observations respectively and b) WRF REF simulation.

Comparisons of the two WRF simulations, forced with (REF) and without (EXP) cool waters in the upwelling area (the resulting SST difference is illustrated by Fig.

SF7b), reveal that during summer the upwelling has local but also large-scale and inter-basin influences on the atmospheric circulation (see 10-meter wind and surface pressure anomalies in Fig. SF7b) and on the precipitation (Fig. SF7c). Upwelling-induced perturbations detailed in the following appear much larger in the EPWP, the GoM, Central America and the Great Plains regions than in the Caribbean Sea itself during summer.

The surface pressure difference between REF and EXP simulations suggests that the upwelling contributes to reduce the surface pressure over the central and eastern United States, while it increases it over the rest of the domain with maximum influence in the southern GoM and Central America, and over the EPWP west of Mexico and California (Fig. SF7b). It may be noted that the anomalous surface pressure dipole induced by the upwelling and centered north and south of the GoM (Fig. SF7b) is consistent with recent works [Kushnir et al., 2010; Feng et al., 2011] showing correlation between warmer-than-normal Atlantic SSTs and reduced rainfall amount over the CONUS and northern Mexico. Here we show that the southern Caribbean upwelling can induce part of this negative SST-rainfall correlation. The cold upwelled waters decrease convection in the western AWP (Figs. SF6a, b), reinforcing the west quadrant of the anticyclonic flow about the NASH that results in anomalous southerlies flowing to CONUS (Fig. SF7b). This leads to a strong convergence anomaly of specific humidity and a slight enhancement of precipitation in the northern half of the GoM states (Fig. SF7c).

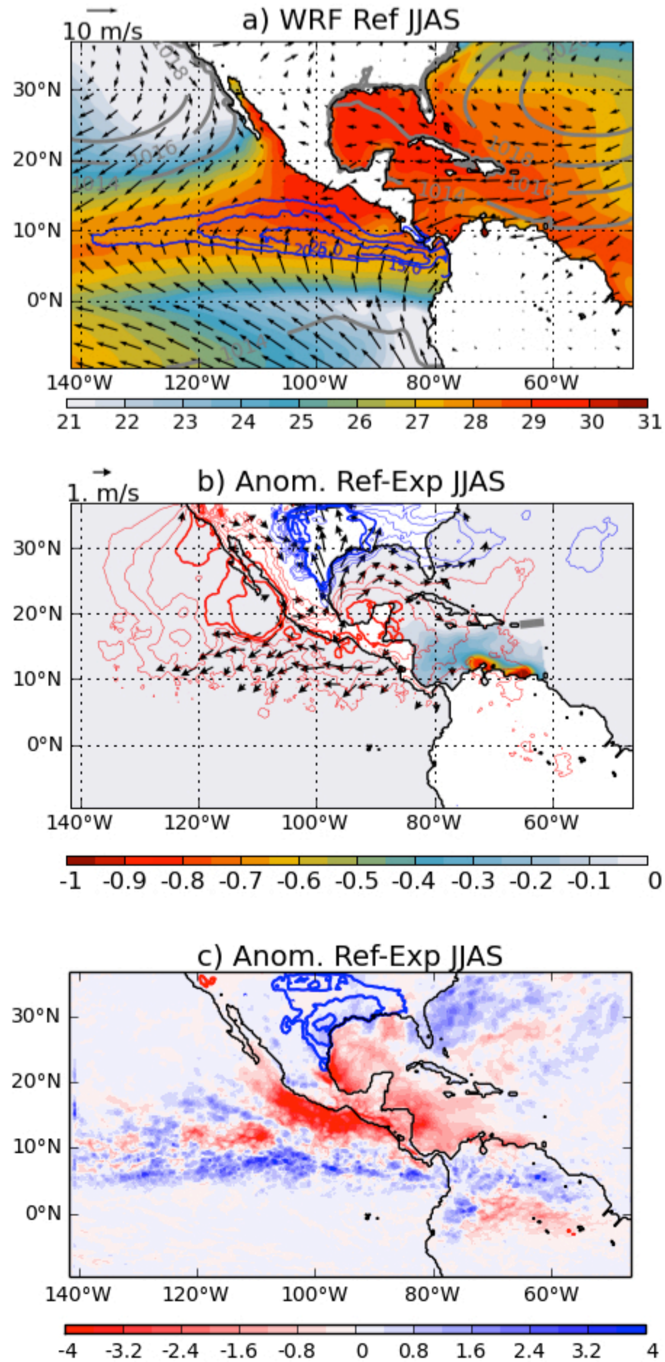

Figure SF7: Mean summer (JJAS) composite (2002-2008) of a) SST [shading; °C], surface pressure [gray contours; hPa], precipitation [blue contours; mm/day] and 10-meter wind [arrows; m/s] from WRF REF simulation. Figures b) to c) show anomaly fields as expressed by (REF - EXP) for b) SST [shading; °C], surface pressure [contours: -0.5 to -0.1 (0.1 to 0.5) in blue (red) with 0.1 increment; hPa], and 10-meter wind [arrows for speed > 0.5; m/s] and c) precipitation [shading; mm/day] with specific humidity [blue (red) contours for positive (negative) +/- 0.001,0.002,0.003 values; kg/kg of air].

S.6 The role of the AWP in steering Atlantic TCs

The AWP also plays an important role in steering TCs in the Atlantic (Wang et al. 2011). An eastward expansion of the AWP has a tendency to shift the location of the cyclogenesis eastward, which reduces the possibility for a TC to make landfall. A large AWP also induces barotropic stationary wave patterns that weaken the NASH and produce the eastward and northeastward TC steering flow anomalies along the eastern seaboard of the United States. Due to these two mechanisms, hurricanes tend to recurve towards the northeast and thereby reducing the chances of making landfall in the southeastern United States. As an example, Wang et al. (2011) find that although both the La Niña event and the large AWP event in 2010 were associated with the increased number of Atlantic TCs, landfalling activity in 2010 was determined by the anomalously large AWP. The following 2011 Atlantic TC season, which was as active as 2010 also featured large AWP and had similar TC track behavior as 2010.

S.7 Ocean barrier layer

Another important process responsible for the barrier layer formation is through the subduction of the salinity maximum water (SMW) in the subtropics of the North Atlantic, which provides a source for the subsurface warm and high-salinity waters in the region (Sprintall and Tomczak, 1992). These barrier layers, when they form during late fall and early winter, weaken entrainment and prevent atmospheric cooling from penetrating into deeper waters. Thus, this region is usually associated with a temperature inversion during the winter (Breugem et al., 2008). The barrier layers persist through the boreal winter due to the seasonal high river runoff from tropical South America and depending on their configuration and persistence into the following spring and summer they can affect tropical cyclone formation and surface biological fields to varying extent. Fig. SF8 shows the extraordinary distribution of riverine surface water in the spring of 2009 as documented by satellite observations (Johns et al. 2014). The northward extension of barrier layers as far north as the U.S. Virgin Islands was confirmed by an *in situ* hydrographic survey (rectangle in Fig. SF8) and is estimated to have not been seen in 30 years. With spring insolation any winter inversions are erased and the layer stability increases, enabling it to survive into summer months when tropical cyclones can be affected by the trapped thermal energy.

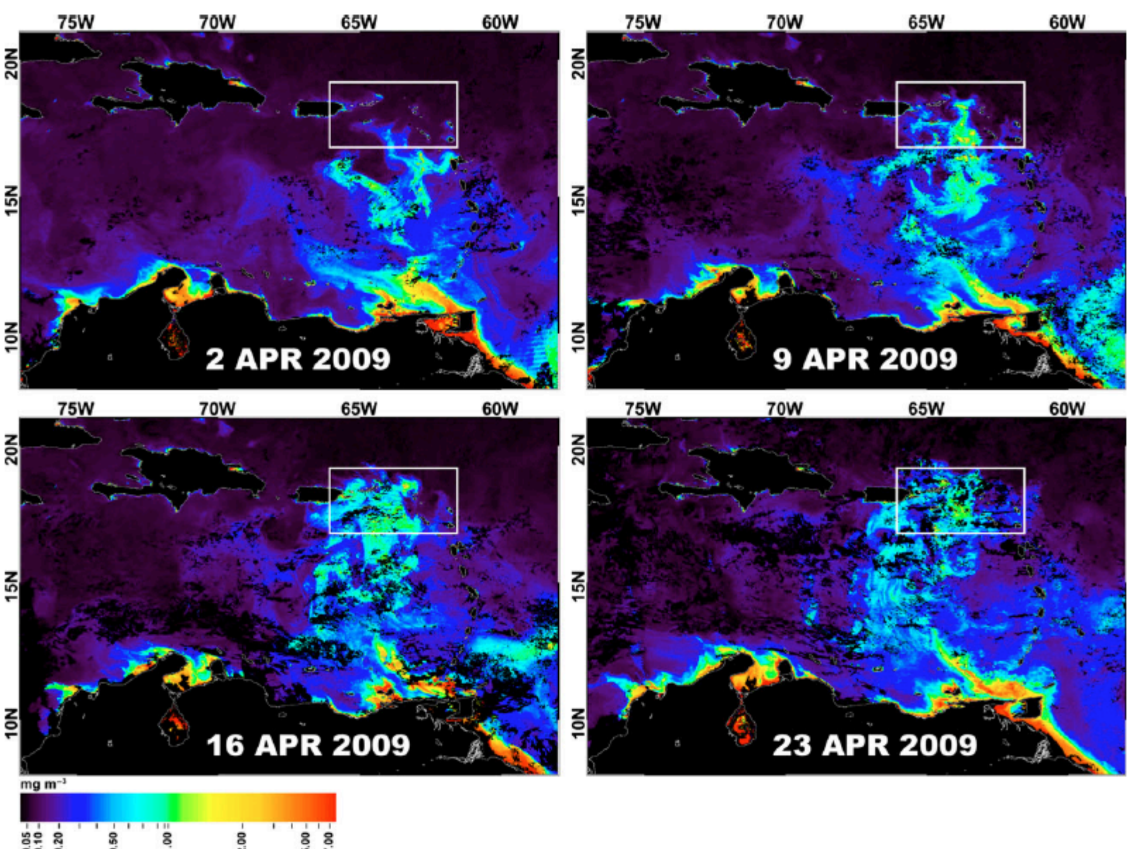

Figure SF8: The composite image of weekly chlorophyll-a concengration (mg m-3)derived from MODIS Terra satellite sensor. Rectangle indicates the area of the hydrographic survey. From Johns et al. (2014).

S.8 The impact of IAS SST bias on convection

Fig. SF9 shows the difference between the joint rainfall-SST PDFs from 27 CMIP5 coupled 20th century simulations (Fig. SF9a) and 27 CMIP5 AMIP simulations (Fig. SF9b) and observations (monthly rainfall from GPCP and SST from HadISST). Coupled CMIP5 historical model simulations produce a SST distribution that is shifted approximately 2°C colder than observed and rainfall is still biased dry (Fig. SF9a). However in atmosphere only AMIP simulations forced by observed SST the rainfall is biased wet (Fig. SF9b). The dominant influence of colder SSTs is clearly evident in the historical joint PDF distribution, with the distribution shifted to the left, or towards colder SST (Fig. SF9a). Due to the cold bias in simulated SSTs of approximately 2°C, the rain rate distribution is shifted to colder SSTs with rain rates biased high at the lower SSTs and biased low at higher SSTs. Overall, the rainfall is underestimated in the coupled simulations due to a reduction of the PDF at all rain rates (a “downward” shift in the PDF in Fig. SF9a when averaged across all SSTs). In the AMIP joint PDF distribution (Fig. SF9b) the increased rainfall for a given SST is evident at all rain rates (shift “upward” toward higher rain rates). This potentially indicates that even if coupled models accurately simulated SST the rainfall distribution would still be incorrect as the atmospheric component of the models overestimated rainfall at observed SSTs.

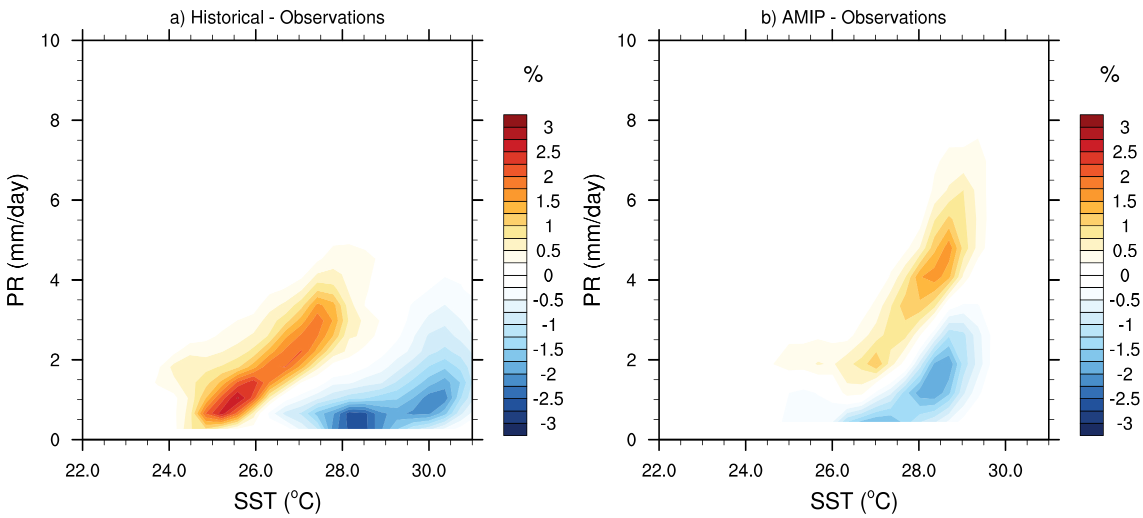

Figure SF9: Joint precipitation rate (PR) – SST PDF distribution differences between historical CMIP5 simulations (a), AMIP CMIP5 simulations (b) and observations for 1979-2005. Cold (warm) colors indicate an underestimation (overestimation) of the frequency of occurrence of a given SST and rainfall amount by the CMIP5 models in comparison to observations.

S.9 The observing network in the IAS region

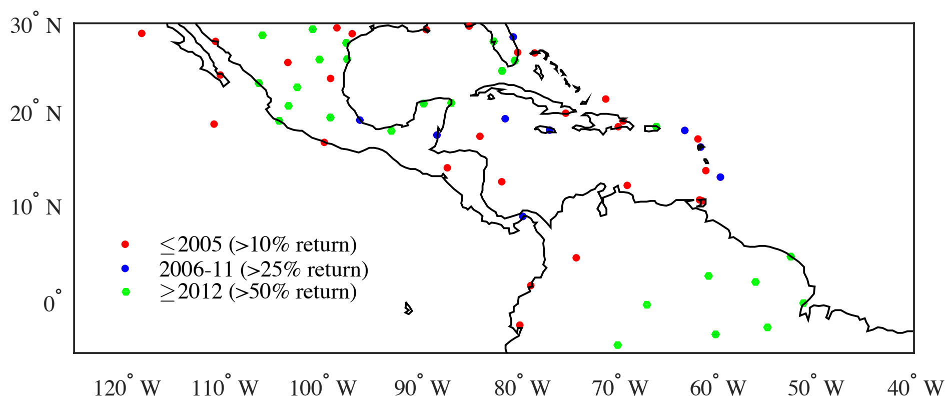

Figure SF10: The network of radiosondes in Latin America that reported at least 10% of their monthly data through 2005, at least 25% of their monthly data between 2006-2011, and at least 50% of their monthly data since 2012.

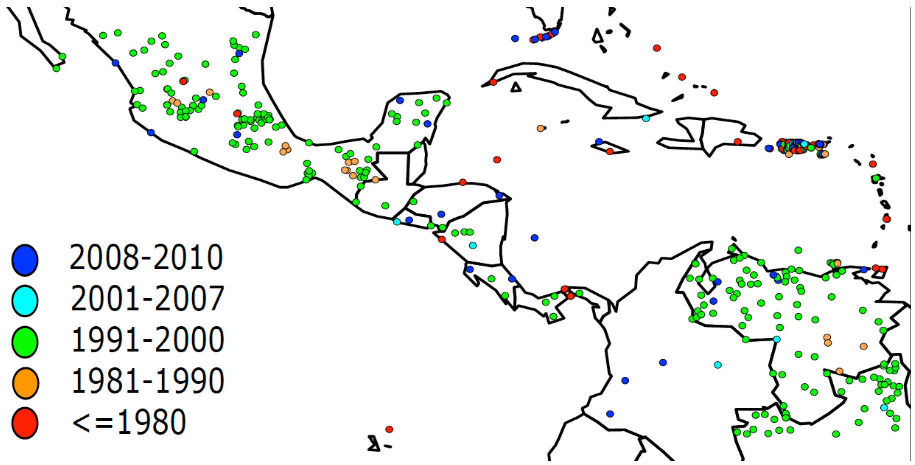

Figure SF11: WMO monthly reporting rainfall stations for the various time intervals indicated in the legend.

S.10 The North American summer seasonal predictability

To highlight the relatively low rainfall forecast skill during the warm season compared to the cold season we show in Fig. SF13 the correlation skill for the NMME system at two months lead verifying in JFM. This figure should be compared with the warm season skill shown in Fig. 14 (main text). The spatial structure of the regions of relatively high skill is different between the warm and cold season, and notably, the correlation is considerably higher during the cold season.

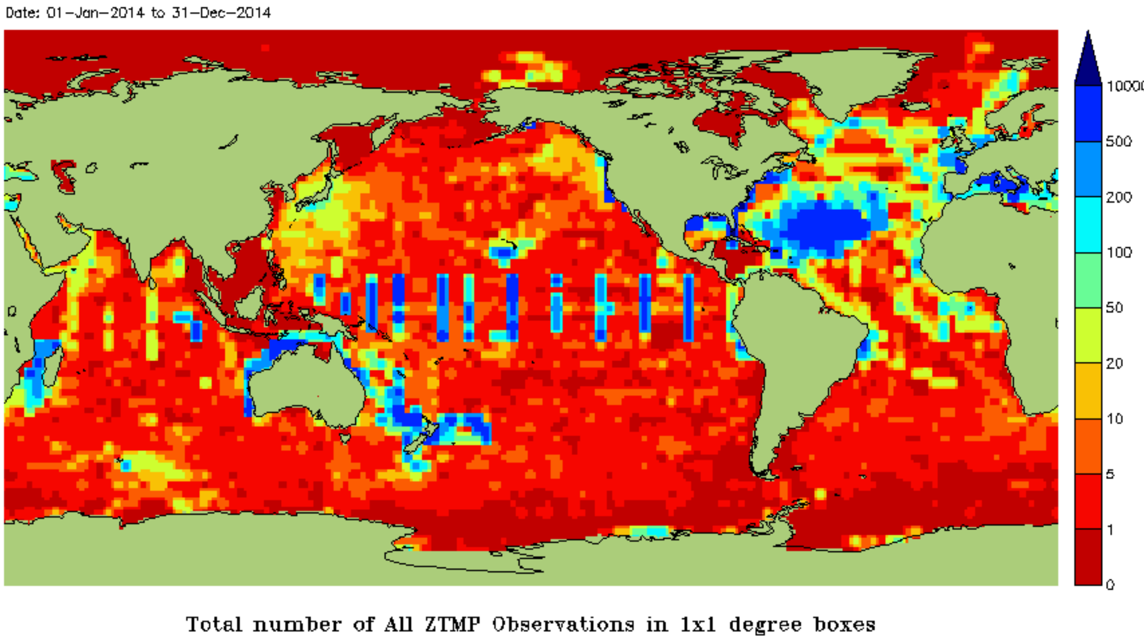

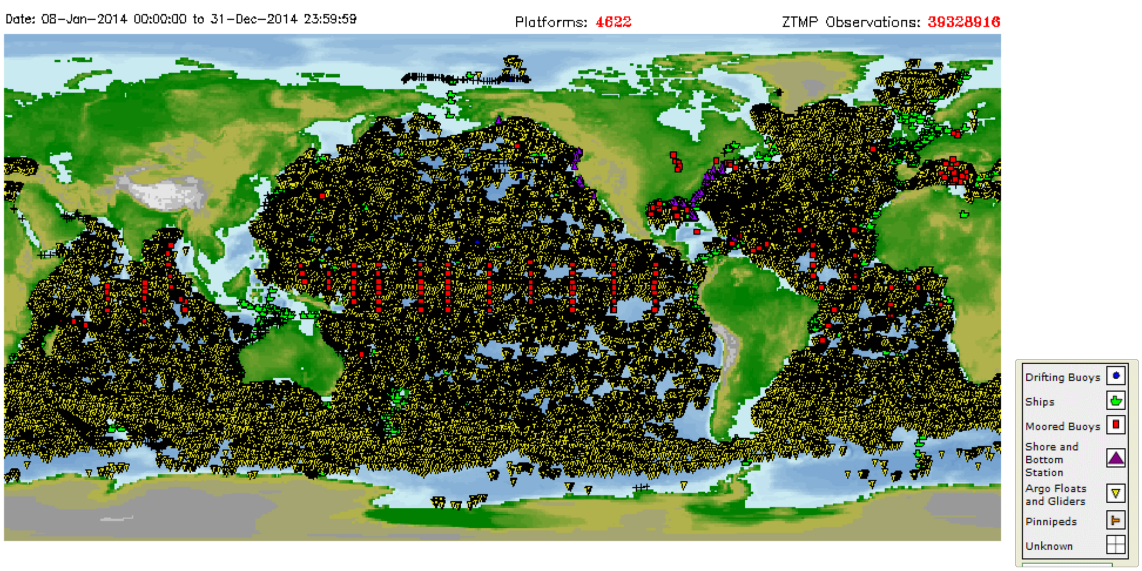

Figure SF12: a) The number of temperature profiles in each 1x1 box for 2014 and b) the location and type of observations used in (a).

Alternatively, we assert that CAPE does have forecast skill – this is because CAPE does not suffer from the vagaries associated with how precipitation is represented in the models, and CAPE tends to be large scale. Of course, predicting CAPE is not the same as predicting rainfall and doesn't directly translate into rainfall. However, variations in CAPE are an indicator of changes in the probability of occurrence of thunderstorms, meso-scale convective systems or extreme rainfall. For example, Figure SF14 shows the contemporaneous correlation between area-averaged CAPE over North America and global SSTA for retrospective forecasts made with CCSM4[1] and observational estimates based on NARR CAPE and TRMM SSTA. Clearly global SSTA contributes to North American CAPE, but variability in the IAS region is of particular importance. The model correlations are somewhat stronger than the observed. This is expected given that the forecasts results are derived from an ensemble mean of ten members. Nevertheless, the IAS region stands out with relatively high correlations in both the model and in the observational estimates.

[1] CCSM4 forecasts are part of the NMME project and follow the retrospective protocol established as part of that project.

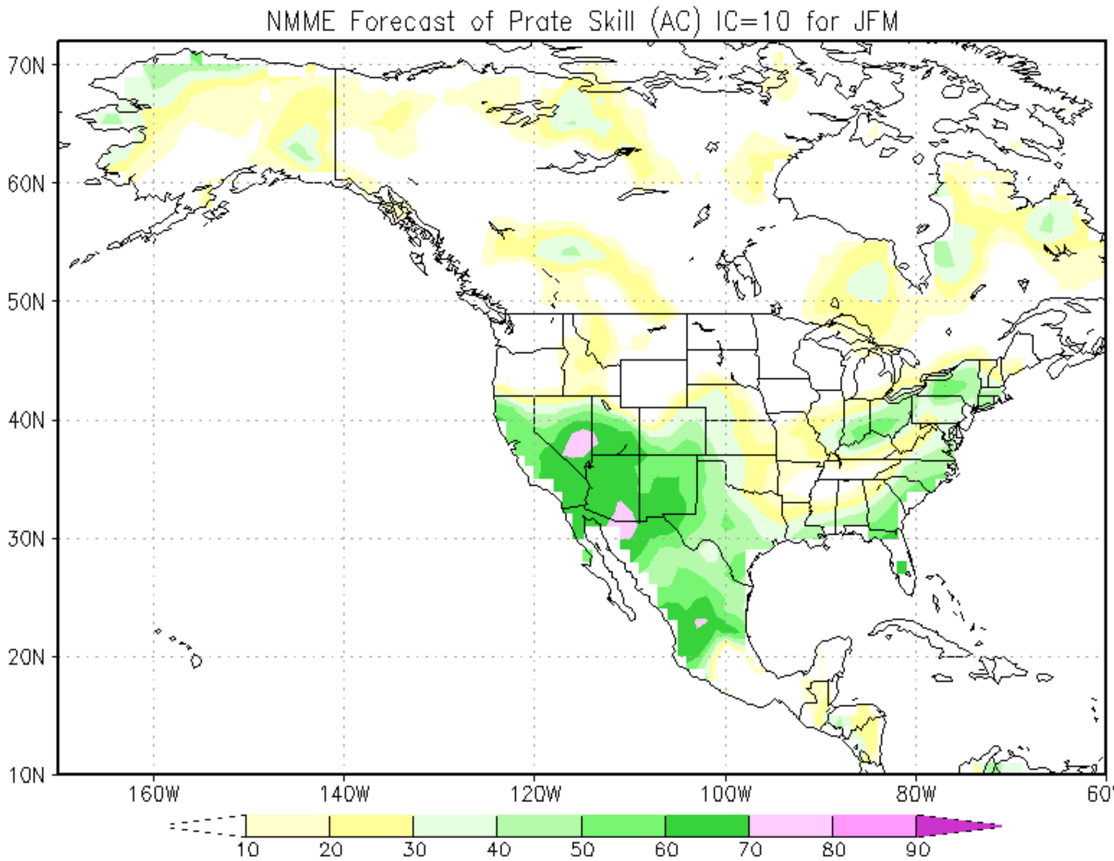

Figure SF13: Anomaly correlation (AC) skill of rainfall prediction for seasonal means of JFM. AC is computed based on the NMME hindcasts over the 1981-2010 period. The NMME initialized in November was used.

These results suggest that there is at least some mechanism for the predictability of North American CAPE during JJA, i.e., slowly evolving SSTA in the IAS region in particular, but also global SSTA. The difficulty is to demonstrate that this potential predictability can be realized in terms of actual forecasts of CAPE, and ultimately shifts in the probability of extreme weather. These are indeed daunting challenges.

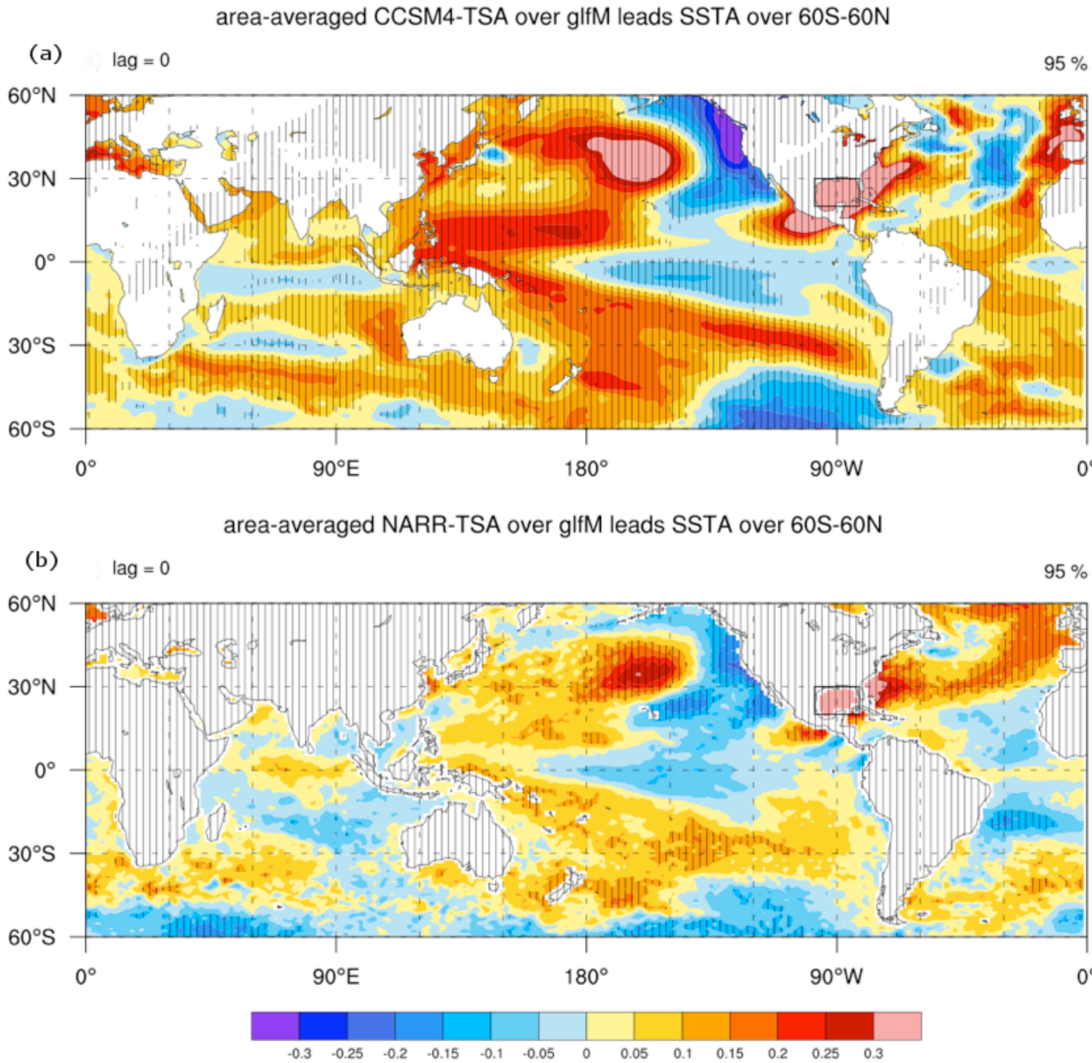

Figure SF14: JJA contemporaneous correlation between SSTA and North American area averaged CAPE for (a) CCSM4 forecasts 1981-2010 initialized in May and (b) observational estimates for CAPE from NARR and SST from TRMM. Hatching over the ocean corresponds to 95% significance.

S.11 Upcoming and new observational programs in IAS and its rim nations

COCONet includes the installation of 50 new continuous Global Navigation Satellite System (cGNSS) and surface meteorology stations in the Caribbean and Central America, refurbishment of an additional 15 stations, and the archival of data from 62 cGNSS stations that are already or will soon be in operation through partnerships with

Caribbean and Central American universities and national agencies. TLALOCNet includes the installation of 24 cGNSS sites, 6 new installations and 18 upgrades to existing stations. Mexican partners, including the National Autonomous University of Mexico (UNAM), will install an additional 13 stations bringing the total to 37 TLALOCNet sites.

Observational networks such as these are helping to fill the gap in observations that exists for both atmospheric and oceanic measurements throughout the IAS and into Mexico. The need for an integrated program of observations and modeling across the IAS is echoed in the Implementation Plan for the Intra-Americas Study of Climate Processes (IASCLiP) and within the World Bank's Modernizing National Meteorological Service to Address Variability and Climate Change in the Water Sector in Mexico (MOMET) project report (Tuluy et al. 2012). The challenge with networks such as COCONet and TLALOCNet, and any future improvements to atmospheric and oceanic observational infrastructure in the region, will be determining how to maintain this infrastructure beyond the project period and how to build the professional and technical capacity within the nations of the IAS to support the infrastructure.